Inertial Attitude and Position Reference System Development for a Small UAV

Dongwon Jung* and Panagiotis Tsiotras†
Georgia Institute of Technology, Atlanta, GA, 30332-0150

This article presents an inexpensive inertial attitude and position reference system for a small unmanned aerial vehicle (UAV) that utilizes low cost inertial sensors in conjunction with a global positioning system (GPS) sensor. The attitude estimates are obtained from a complementary filter and a Kalman filter by combining the measurements from the inertial sensors with the supplementary attitude information from GPS. A method is proposed to deal with the GPS data latency and momentary outages. The inertial position is estimated from a separate Kalman filter that is cascaded after the attitude filters in order to reduce the computational overhead. Numerical simulation results and hardware validation show that this is a simple, yet effective method for attitude and position estimation, suitable for real-time implementation on a small UAV.

I. Introduction

Control of unmanned aerial vehicles (UAVs) requires increased automation from the top level (trajectory design and planning) to the bottom level (stabilization and tracking) of the control architecture hierarchy. Most important in this hierarchy, is to know the correct states of the vehicle, such as orientation, absolute position, and so on. Most UAVs are equipped with various sensors to correctly measure the state variables, so state estimation has become indispensable in modern strapdown navigation systems.

A number of estimation filters has been proposed since 1970s. The basic idea is to blend several different measurements to obtain the best approximation of the signals. Among these filters, the Kalman filter has been widely used for attitude determination.[1,2,3] The Kalman filter provides the best estimates based on the system dynamics and a priori knowledge of the noise characteristics of the signals. Major difficulties when implementing a Kalman filter on a micro-controller arise from the complexity caused by the need of inverting certain matrices. This problem is exacerbated by the need to implement an extended Kalman filter (EKF) in case the system is nonlinear and with a large number of states. In contrast to the Kalman filter, the complementary filter is simple, easy to implement, and has been successfully used for decades on a low-performance micro-controllers.[4,5]

The strapdown attitude determination problem solves for the three-axis attitude of the vehicle by utilizing onboard inertial sensors such as rate gyros, accelerometers, and magnetometers. It is known that two non-parallel vector measurements of an inertial fixed vector from strapdown sensors enable one to compute the three-axis attitude by incorporating sophisticated numerical schemes.[6,2,7] Such algorithms approximate the inertial angles from body-fixed measurements. On the other hand, since GPS can provide direct measurements with respect to the inertial frame, several authors have proposed employing GPS sensors to extract the attitude information from GPS measurements.[8,9,10] The GPS sensor provides unbiased measurements at centimeter level accuracy, and the direct use of GPS in attitude estimation avoids complex computations. This approach has been successfully applied to small UAVs.[11]

The GPS output has a low update rate compared to the update rate of other inertial sensors. As a result, difficulties arise when one needs the absolute position at high rates for use within the navigation loop. For a high rate navigation solution, the GPS should be supplemented by a set of inertial sensors. A complete and very accurate navigation solution can be achieved by an estimation filter in which the attitude states

*Graduate student, School of Aerospace, dongwon_jung@ae.gatech.edu, AIAA student member.
†Professor, tsiotras@gatech.edu, AIAA Member.

and the navigation states are tightly coupled.[12] This combination provides a complete navigation solution for all ranges of operation, but it is not suitable for implementation on a micro-controller due to its high filter dimension. In contrast, an appropriate combination of GPS and inertial sensors provides an alternative choice for reducing the computational burden. In this configuration, the GPS serves as an independent sensor suite providing position measurements to an estimation filter that also utilizes the attitude estimates from a separate filter.[13] It turns out that this approach is simple and straightforward to implement, but an algorithm needs to handle spurious outputs owing to the measurement latency and, on certain occasions, GPS outage.

This article presents a low cost inertial attitude and position reference system for a small UAV, which is comprised of two separate estimation filters for attitude and position. The estimation algorithms are simple, yet effective so that a micro-controller can execute these algorithms within a small time interval. In the following, an algorithm that combines a complementary filter and a Kalman filter is developed for the Euler attitude angles, and an inertial sensor suite is adopted to combine its output with the GPS output. A straightforward and innovative way of handling the data latency and the outage of a GPS sensor is introduced. Finally, a cascaded position estimation Kalman filter is designed utilizing the attitude estimates to lower the computational burden with a small performance loss. The filters are tested in a hardware-in-the-loop (HIL) environment to verify the feasibility of the algorithms, and are implemented on an autopilot which is equipped with a micro-controller and sensors.

II. Attitude estimation

The sensors involved in a strapdown attitude and heading reference system are rate gyros, accelerometers and magnetometers. These sensors measure the three-axis angular rates, three-axis apparent acceleration (gravity minus inertial acceleration), and Earth's magnetic field with respect to the body frame. In order to obtain the best estimate of the attitude angles from the available sensors, it is imperative to blend these measurements in a seamless manner by taking into account the different signal specifications for each sensor.

II.A. Complementary filter

Complementary filters have been widely used to combine two independent noisy measurements of the same signal, where each measurement is corrupted by different types of spectral noise.[4] The filter provides an estimate of the true signal by employing two complementary high-pass and low-pass filters. Figure 1(a) shows the case of a complementary filter to obtain an estimate $\hat{x}(t)$ of $x(t)$ from the two measurements $x_m(t)$ and $\dot{x}_m(t)$. Notice that $x_m(t)$ is the measurement of the signal with predominantly high-frequency noise $n_1(t)$, and $\dot{x}_m(t)$ is the measurement of the rate of change of the signal with low-frequency noise $n_2(t)$ as follows

$$x_m(t) = x(t) + n_1(t) \quad \text{and} \quad \dot{x}_m(t) = \dot{x}(t) + n_2(t). \tag{1}$$

From Fig. 1(a), it is apparent that the Laplace transform of the estimate of $x(t)$ can be written as

$$\hat{X}(s) = \underbrace{\frac{1}{\tau s+1}X(s) + \frac{\tau s}{\tau s+1}X(s)}_{\text{Signal terms}} + \underbrace{\frac{1}{\tau s+1}N_1(s) + \frac{\tau s}{\tau s+1}\left(\frac{1}{s}N_2(s)\right)}_{\text{Noise terms}}. \tag{2}$$

The noise terms in both channels are effectively suppressed by the first order low- and high- pass filter with the time constant τ. The frequency response plot shown in Fig. 1(c) illustrates the contribution of each frequency channel to the output, where the cutoff frequency is chosen as 1 rad/sec. The time constant τ is selected according to the noise characteristics of each channel such that the estimate $\hat{x}$ is contributed by integration of $\dot{x}_m$ over frequencies $\omega \gg 1/\tau$, whereas for frequencies $\omega \ll 1/\tau$, $\hat{x}$ tracks x_m. At frequencies near $1/\tau$ the estimated output $\hat{x}$ is a combination of the two channels, which appears as a hump in Fig. 1(c). The estimate approximates the true signal faithfully over most of the frequency range.

In order to implement a complementary filter on a micro-controller, a discrete version of the high-pass and low-pass filters should be written in software by taking into consideration the sampling period of the micro-controller. The filter coefficients for the discrete filters are related to the time constant τ, which forces the user to recalculate the coefficients of both filters, if necessary. Instead, an alternative form of the complementary filter can be used as depicted in Fig. 1(b). The filter transfer function remains the same as in Eq. (2) but the feedback structure of the filter simplifies the filter implementation on a micro-controller. It

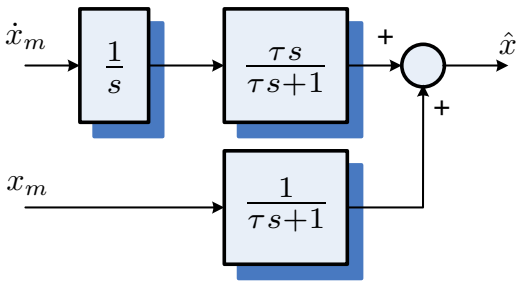

(a) Direct complementary filter

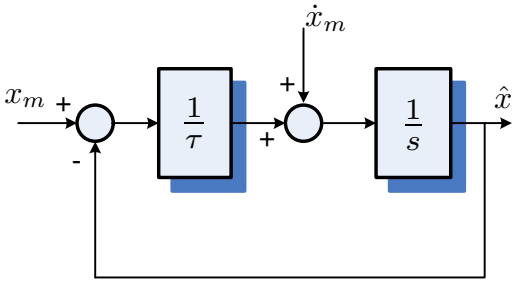

(b) Indirect complementary filter

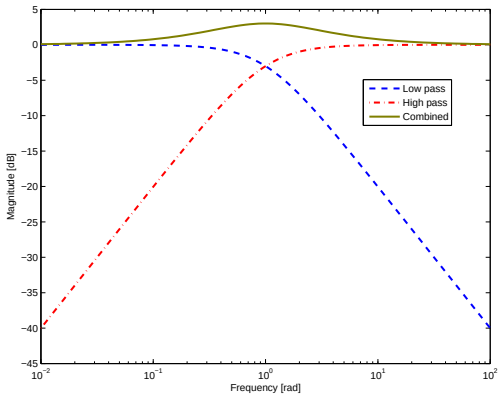

(c) Frequency magnitude plot of the complementary filter

Figure 1. Two different schemes for the implementation of the complementary filter.

also allows easy tuning for acceptable performance when low cost sensors are used. In addition, this feedback structure can be easily adapted to deal with multiple measurements. Figure 2 illustrates the case when using two low frequency channels. A tuning parameter $\alpha_k \in [0, 1]$ sets the relative weight between the signals x_{m_1} and x_{m_2}. In this manner the filter takes advantage of multiple measurements to obtain the best estimate.

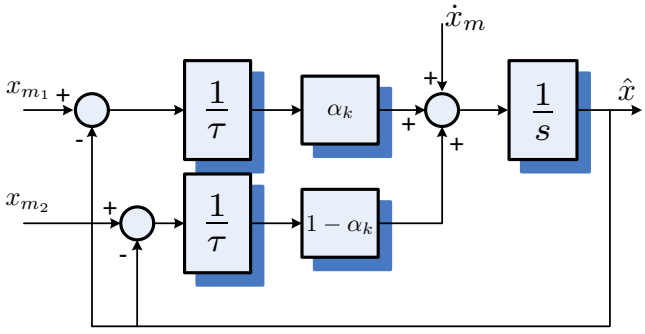

Figure 2. Multiple measurement augmentation in the indirect complementary filter.

II.B. Pitch and heading angle estimation

The low frequency dominant pitch angle is directly calculated from the accelerometer output because the accelerometer is able to measure the gravity vector minus the inertial acceleration (the apparent acceleration, $\vec{g} - \vec{a}_I$) with respect to the body axes. In a steady state flight condition, specifically at a constant altitude level flight, the accelerometers yield mostly the gravity vector since the inertial acceleration is negligible in

this case. Then the pitch angle is calculated from the acclerometer output $\mathbf{a} = [a_x \; a_y \; a_z]^\mathsf{T}$ as follows

$$\theta_L = -\sin^{-1}\left(\frac{a_x}{g}\right). \tag{3}$$

The low frequency dominant heading angle is determined by two different sources: the GPS sensor and the magnetometer. The GPS sensor used in this work provides an absolute heading information ψ_{GPS} at a low rate (1 Hz), whereas the output of the three-axis magnetometer $\mathbf{m} = [m_x \; m_y \; m_z]^\mathsf{T}$ with respect to the body axes provides a heading measurement ψ_L at a much higher rate according to the following relationship[14]

$$\psi_L = \begin{cases} \pi - \tan^{-1}(\bar{m}_y/\bar{m}_x) & \text{if } \bar{m}_x < 0, \\ 2\pi - \tan^{-1}(\bar{m}_y/\bar{m}_x) & \text{if } \bar{m}_x > 0,\ \bar{m}_y > 0, \\ -\tan^{-1}(\bar{m}_y/\bar{m}_x) & \text{if } \bar{m}_x > 0,\ \bar{m}_y < 0, \\ \pi/2 & \text{if } \bar{m}_x = 0,\ \bar{m}_y < 0, \\ 3\pi/2 & \text{if } \bar{m}_x = 0,\ \bar{m}_y > 0, \end{cases} \tag{4}$$

where $\bar{m}_x$ and $\bar{m}_y$ are the projected magnetic field components on the horizontal plane that can be calculated by transforming $\mathbf{m}$ through the rotation matrix $\mathcal{C}(\phi,\theta) \triangleq \left(\mathcal{C}_1(\phi)\mathcal{C}_2(\theta)\right)^\mathsf{T}$. If the pitch angle θ and the roll angle ϕ are not available, their estimates $\hat{\theta}$ and $\hat{\phi}$ can be used instead, to yield

$$\begin{aligned} \bar{m}_x &= m_x \cos\hat{\theta} + m_y \sin\hat{\phi}\sin\hat{\theta} + m_z \cos\hat{\phi}\sin\hat{\theta}, \\ \bar{m}_y &= m_y \cos\hat{\phi} - m_z \sin\hat{\phi}. \end{aligned} \tag{5}$$

The high frequency dominant pitch and heading angles are inferred from the attitude kinematics equations,

$$\begin{aligned} \dot{\theta} &= q\cos\hat{\phi} - r\sin\hat{\phi}, \\ \dot{\psi} &= (q\sin\hat{\phi} + r\cos\hat{\phi})/\cos\hat{\theta}, \end{aligned} \tag{6}$$

where $\boldsymbol{\omega} = [p \; q \; r]^\mathsf{T}$ is the onboard rate gyro measurement.

Figure 3 illustrates the block diagram of the combined complementary filters for pitch and heading angle estimation. As discussed earlier, the filters can be tuned for acceptable performance via the parameters τ_θ and τ_ψ for pitch and heading angle, respectively. The relative weight between the heading angles from either the magnetometer or the GPS sensor is imposed by a parameter $\alpha_\psi \in [0\ ,1]$ in order to put more emphasis on the measurement that seems to be close to the true heading. A detailed description regarding the adaptive tuning of α_ψ is given later in the paper.

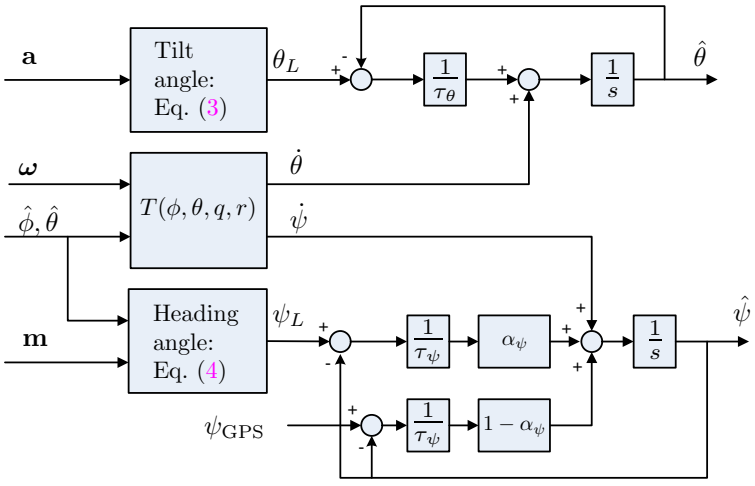

Figure 3. Entire complementary filter setup for pitch and heading angles.

II.C. Roll angle estimation

The roll angle can also be estimated from a complementary filter using high frequency dominant information from $\dot{\phi}$ via the attitude kinematics and low frequency dominant information from the kinematic relationship of the airplane at a banked condition. As illustrated in Fig. 4, if an airplane is in a purely banked, coordinated

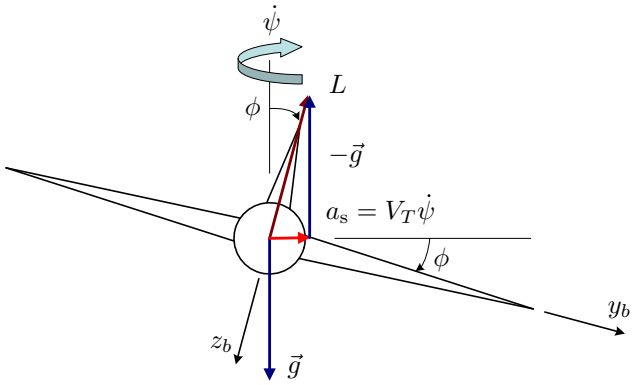

Figure 4. Kinematic relationship at a truly banked turn condition.

turn condition (no side acceleration along body y-axis), then the roll angle is approximately computed by the following equation assuming no wind,[15]

$$\sin\phi = \frac{\dot{\psi}V_T}{g}, \tag{7}$$

where V_T is the flight speed and g is the gravitational acceleration. This equation can be further approximated using $\sin\phi \approx \phi$ and $\dot{\psi} \approx r$ as

$$\phi = \frac{rV_T}{g}. \tag{8}$$

Then the low frequency dominant roll angle is approximated from Eq. (8) with the yaw rate from the yaw gyro and the flight speed from a pitot tube. In practice, the estimate of Eq. (8) tends to be biased since it utilizes directly the gyro output r which is vulnerable to drift. Over a long period of time the estimate will deviate owing to this yaw rate bias.[5] To compensate for this bias, a Kalman filter was designed as follows.

In general, the fast roll dynamics of the airplane allows us to use a linear approximation for the roll kinematics $\dot{\phi} = p$. The roll rate gyro measurement p_m is assumed to be corrupted by the roll rate bias p_b as well as measurement noise η_p,

$$p_m = p + p_b + \eta_p.$$

The biases for both roll and yaw gyros are modelled as random walk processes driven by Gaussian white noise processes. It follows that the equations of the filter dynamics are given by

$$\begin{aligned} \dot{\phi} &= p_m - p_b - \eta_p, \\ \dot{p}_b &= \epsilon_p, \\ \dot{r}_b &= \epsilon_r. \end{aligned} \tag{9}$$

The measurement model of the Kalman filter includes the yaw gyro output and the rate of heading angle change related to the heading angle measurement from the GPS sensor. The yaw rate gyro measurement r_m contains a bias r_b and measurement noise η_r,

$$r_m = r + r_b + \eta_r. \tag{10}$$

Here the yaw rate measurement can be related to the roll angle, using Eq. (8), as follows

$$r_m = \frac{g}{V_T}\phi + r_b + \eta_r. \tag{11}$$

On the other hand, because the GPS sensor provides the heading angle at one second intervals, the rate of the heading angle change $\dot{\psi}$ is calculated through numerical differentiation. It follows from Eq. (7) that

$$\dot{\psi}_m = \frac{g\cos\hat{\phi}}{V_T^*}\phi + \eta_{\dot{\psi}}, \tag{12}$$

where V_T^* is the flight speed obtained from the GPS sensor and $\eta_{\dot{\psi}}$ is the measurement noise. Equations (11) and (12) become the measurement model for the roll angle Kalman filter. The Kalman filter is implemented in a discrete format on the micro-controller using a sampling period Δt:

- **Time update**
  - Project ahead

$$\begin{aligned} \hat{\mathbf{x}}_k^- &= \Phi_k \hat{\mathbf{x}}_{k-1} + \begin{bmatrix} \Delta t p_m^k & 0 & 0 \end{bmatrix}^\mathsf{T}, \\ \mathbf{P}_k^- &= \Phi_k \mathbf{P}_{k-1} \Phi_k^\mathsf{T} + \mathbf{Q}_k, \end{aligned} \tag{13}$$

    where,

$$\Phi_k = \begin{bmatrix} 1 & -\Delta t & 0 \\ 0 & 1 & 0 \\ 0 & 0 & 1 \end{bmatrix}, \qquad \hat{\mathbf{x}}_k = \begin{bmatrix} \hat{\phi}_k \\ \hat{p}_{b_k} \\ \hat{r}_{b_k} \end{bmatrix}.$$

- **Measurement update**
  - Compute Kalman gain

$$\mathbf{K}_k = \mathbf{P}_k^- \mathbf{H}_k^{\star\mathsf{T}} \left(\mathbf{H}_k^\star \mathbf{P}_k^- \mathbf{H}_k^{\star\mathsf{T}} + \mathbf{R}_k^\star \right)^{-1}, \tag{14}$$

  - Update estimate with measurements

$$\hat{\mathbf{x}}_k = \hat{\mathbf{x}}_k^- + \mathbf{K}_k (\mathbf{z}_k^\star - \mathbf{H}_k^\star \hat{\mathbf{x}}_k^-), \tag{15}$$

  - Compute error covariance for updated estimate

$$\mathbf{P}_k = (\mathbf{I} - \mathbf{K}_k \mathbf{H}_k^\star) \mathbf{P}_k^-, \tag{16}$$

    where, $\star = s,\ f$.

Note that the measurement update for GPS is done once every second, when the new $\dot{\psi}_m$ becomes available, whereas the measurement update for the yaw rate gyro takes places at a high update rate. These two measurement updates are coordinated such that each update is completed whenever the corresponding measurement becomes available: a fast update for r_{m_k} and a slow update for $\dot{\psi}_{m_k}$, as follows

- Fast update

$$\mathbf{z}_k^f = r_{m_k}, \qquad \mathbf{H}_k^f = \begin{bmatrix} \dfrac{g}{V_T} & 0 & 1 \end{bmatrix}, \tag{17}$$

- Slow update

$$\mathbf{z}_k^s = \dot{\psi}_{m_k}, \qquad \mathbf{H}_k^s = \begin{bmatrix} \dfrac{g}{V_T}\cos\hat{\phi}_k^- & 0 & 1 \end{bmatrix}. \tag{18}$$

The process noise covariance matrix $\mathbf{Q}_k$ and measurement noise covariance matrix $\mathbf{R}_k$ are determined from the noise characteristic of each signal, as follows

$$\begin{aligned} \mathbf{Q}_k &= \mathrm{diag}\Big(E\big[\begin{array}{ccc} \bar{\eta}_p^2 & \bar{\epsilon}_p^2 & \bar{\epsilon}_r^2 \end{array} \big] \Big), \\ \mathbf{R}_k^f &= E\big[\bar{\eta}_r^2\big], \qquad \mathbf{R}_k^s = E\big[\bar{\eta}_{\dot{\psi}}^2\big], \end{aligned} \tag{19}$$

where the overbar variables represent the discrete noise sequences at the sampling period of Δt such that they have equal noise strength as the continuous noise processes, and $E[\cdot]$ calculates the mean-square noise strength. The noise covariance matrices $\mathbf{Q}_k$ and $\mathbf{R}_k$ are computed from the noise characteristic of each sensor assuming that the noise processes are uncorrelated to each other.

II.D. Dealing with GPS latency and GPS lock

The GPS sensor employed in this research has an inherent data latency, which causes the output of the GPS sensor to be delayed by a certain amount of time. The position and velocity output from the GPS sensor at the kth time step are calculated internally based on the satellite range measurements at the epoch of the $(k-1)$th time step. Combining the latency due to the internal data processing along with the communication latency, the time delay of the position output is observed to be about 0.1 sec and the delay of the velocity output about 1.1 sec.[16] The GPS sensor provides the heading angle based on the velocity output, so the measurement of ψ_{GPS} is also delayed by 1.1 sec. Unless this delay is properly compensated, substantial errors will arise during the estimation process.

Figure 5 illustrates graphically the issue of delay. Assume that the measurement is delayed by N samples. Then the measurement $\mathbf{z}_k^*$ at $t = t_k$ represents the states of the N prior sample $\mathbf{z}_k^* = \mathbf{H}_{k-N}^s \mathbf{x}_{k-N}$. Several arrangements to incorporate delays into the Kalman filter framework have been suggested in the literature.[17,18] One approach is to simply recalculate the complete time-trajectory of the filter throughout the delayed period when a delayed measurement is received. The large memory cost for storing the intermediate states over the delayed period and the associated increased computational cost forbid delayed measurements to be incorporated directly in a real-time estimation algorithm. Another approach to account for delayed

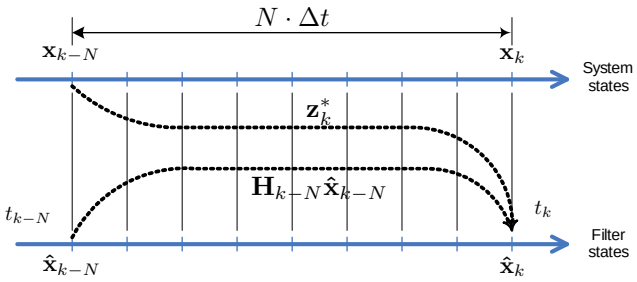

Figure 5. System with a delayed measurement due to sensor latency.

measurements is to make use of the state estimate corresponding to the delayed measurement at $t = t_{k-N}$, i.e., $\hat{\mathbf{x}}_{k-N}$ in a buffer. When the delayed measurement $\mathbf{z}_k^*$ becomes available at the time $t = t_k$, an innovation that is calculated from the delayed measurement and the delayed state estimate in the buffer is blended with the current estimate state in the standard Kalman measurement update as follows

$$\hat{\mathbf{x}}_k = \hat{\mathbf{x}}_k^- + \mathbf{K}_k(\mathbf{z}_k^* - \mathbf{H}_{k-N}^s \hat{\mathbf{x}}_{k-N}). \tag{20}$$

Compared to the case of a wrong innovation calculated from the delayed measurement and the current state estimate $\hat{\mathbf{x}}_k^-$ (no delay compensation), this approach forces the correct innovation to be used in the measurement update and then yields a better estimate. Nonetheless, this is a sub-optimal solution.[18]

The estimation filters presented in the previous section assumed that the GPS measurement is always available. However, the GPS output is locked when a GPS outage occurs, failing to provide continuous information. The situation gets even worse if the UAV performs aggressive motions such as a sharp turn at high speed. During such an outage, the GPS output is held at the last valid output. Figure 6 demonstrates the real measured GPS data when the UAV performs a sharp turn by a remote pilot. The plot shows that at $t = 2711.2$ sec the GPS heading angle is held to the previous value of -90 deg. The value is kept until $t = 2714.2$ sec when a new (possibly valid) heading angle is provided by the GPS sensor. Because the attitude estimation algorithm presented earlier utilizes the heading angle measurement from the GPS sensor, an incorrect heading information from the GPS sensor due to a GPS outage would result in a wrong estimation of the heading angle from the complementary filter. Moreover, this would lead to a wrong estimation of the roll angle from the Kalman filter.

One possible remedy to this is to use intermittently the heading information from the magnetic compass for a short time period (i.e., during GPS outage). Even though any local magnetic distortion due to existence of ferrous materials near the magnetic compass yields a small offset in the magnetic heading information, the magnetic heading information can provide continuous heading measurement to the filtering algorithm even when a GPS outage occurs. Whenever the complementary filter detects the GPS heading angle being held constant, it first modifies the weight parameter α_ψ to put more emphasis on the magnetic heading

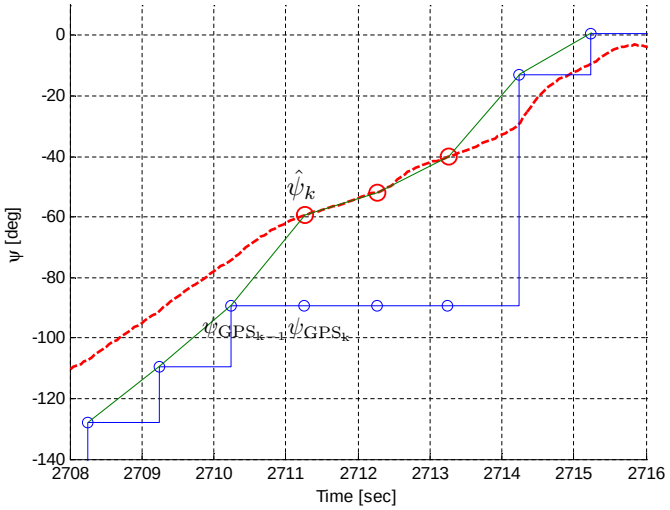

Figure 6. GPS momentary outage during an aggressive maneuver.

information. As the α_ψ approaches one, the magnetic heading information is used more exclusively in the complementary filter, while the GPS heading information is ignored. The adaptive tuning of α_ψ is done by

$$\alpha_\psi^* = \alpha_\psi + (1 - \alpha_\psi)\lambda \tag{21}$$

where, $\lambda \geq 1$ controls the rate of change of weight parameter. Once the GPS is back to normal operation, the weight parameter will restore the specified value for a normal operation. After the complementary filter computes the heading estimate during a GPS outage, the Kalman filter can make use of the heading estimate from the complementary filter in order to obtain the rate of change of the heading angle in Eq. (18). Figure 6 describes the use of heading estimate from the complementary filter to compute the rate of change of the heading angle during a GPS outage. Notice that at $t = 2711.2$ sec, a GPS outage occurs and the heading angle is held fixed. Then the Kalman filter switches to using the heading estimate $\hat{\psi}_k$ instead of the false heading $\psi_{\mathrm{GPS_k}}$ to calculate

$$\dot{\psi}_k^* = (\hat{\psi}_k - \psi_{\mathrm{GPS}_{k-1}}). \tag{22}$$

The use of the estimated heading continues until the GPS sensor gives correct heading information at $t = 2714.2$ sec.

II.E. Attitude filter validation

The previous algorithm was written in C code and implemented as an S-function in the Matlab/Simulink® environment. This enables the C code to be validated for any errors and tuned before using it on the autopilot. A complete non-linear 6-DOF Simulink model[19] is used to simulate the full dynamics of the UAV. The inertial sensor measurements are emulated to have close correlation to the real sensors used in the UAV in terms of signal specification and noise characteristics. The gain parameters for the pitch and heading complementary filters were chosen as

$$\tau_\theta = 2, \quad \tau_\psi = 0.5, \quad \alpha_\psi = 0.4.$$

The process noise covariance matrix and the noise covariance matrix for the Kalman filter were carefully chosen in consideration of the noise characteristics of the sensors as follows

$$\begin{aligned} \mathbf{Q}_k &= \mathrm{diag}\Big(\begin{bmatrix} 0.02^2 & 0.001^2 & 0.01^2 \end{bmatrix}\Big), \\ \mathbf{R}_k^f &= 0.02^2, \qquad \mathbf{R}_k^s = 0.05^2. \end{aligned} \tag{23}$$

Two internal PID controller loops were designed for roll angle control and pitch angle control with the associated stability augmentation dampers. The filter outputs are fed back to the corresponding PID

controllers and validated in the closed loop. Figure 7 shows the comparison between true values and estimated values. In Figs. 7(a) and 7(c) a doublet roll angle reference command was used to excite the lateral motion of the airplane, while the pitch angle is held constant at zero. Both the complementary filter and the Kalman filter function appropriately. Nonetheless, a transient time lag in the estimation process is observed when the UAV changes its orientation quickly, and this aspect leads to the increased estimation error shown in the right side of Figure 7 during the transients. The low bandwidth output of the GPS sensor causes the latency of the estimation with respect to the fast motion, however, the filter converges to the correct angle after the UAV comes into steady state. Figure 7(b) shows the pitch angle estimation when a doublet pitch angle reference command was used to excite the longitudinal motion of the UAV, while the roll angle is controlled to zero.

III. Position Estimation

In this section a filter for estimating the absolute position of the UAV in the north-east-down (NED) inertial reference frame is developed. A typical attitude heading reference system/inertial navigation system (AHRS/INS) makes use of the accelerometer output in conjunction with the full equations of motion to propagate the inertial position and velocity from acceleration measurements using a Kalman filter. However, the dimension of the Kalman filter is too large to be implemented on a micro-controller and execute in real-time. Instead of using the full equations of motion, the navigation equations are used to propagate the position from flight speed measurements. The position filter is cascaded to the attitude filters so as to allow separate filter tuning and at the same time to reduce the computational cost with minimal loss of performance.

III.A. Filter formulation

The navigation equations of a 6-DOF airplane[20] are used to obtain the position filter equation. Using the transformation matrix from the body axes ($\mathcal{B}$) to the inertial frame ($\mathcal{N}$),

$$\begin{bmatrix} \dot{p}^N \\ \dot{p}^E \\ \dot{p}^D \end{bmatrix} = \begin{bmatrix} v^N \\ v^E \\ v^D \end{bmatrix} = \left[{}^{\mathcal{B}}\mathbf{C}^{\mathcal{N}} \right]^{\mathsf{T}} \begin{bmatrix} U \\ V \\ W \end{bmatrix}, \tag{24}$$

where ${}^{\mathcal{B}}\mathbf{C}^{\mathcal{N}}$ is the rotation matrix using 3(ψ)-2(θ)-1(ϕ) Euler angles. Assume that the angle of attack and side slip angle are small, the velocity components expressed in body axes are approximated by

$$U \approx V_T, \qquad V, W \approx 0. \tag{25}$$

The flight speed V_T, if it is measured from a pitot tube, includes the inertial speed (relative ground speed) and the wind speed. The relative ground speed is only to be integrated to propagate the inertial position. The wind speed is dependent on the flight condition, so is added to the position filter as an extra state to account for the pitot speed measurement. A random walk model for the wind speed variation is assumed, driven by a Gaussian white noise process as follows

$$\dot{V}_w = \epsilon_w. \tag{26}$$

The speed measurement V_{T_m} from the pitot tube contains the inertial speed, the wind speed, and the measurement noise η_w,

$$V_{T_m} = V_T + V_{\mathrm{w}} + \eta_w. \tag{27}$$

The attitude angle information used in Eq. (24) is provided separately by the attitude filters. This cascaded configuration of the attitude and position filters reduces the complexity arising from the coupling of the variables. It therefore yields a simple position estimation filter with minimal order. It follows from Eq. (24), (25), and (27) , that the equations of filter dynamics are given by

$$\begin{bmatrix} \dot{p}^N \\ \dot{p}^E \\ \dot{p}^D \\ \dot{V}_w \end{bmatrix} = \begin{bmatrix} \cos\theta\cos\psi \\ \cos\theta\sin\psi \\ -\sin\theta \\ 0 \end{bmatrix} (V_{T_m} - V_w) + \begin{bmatrix} \nu_N \\ \nu_E \\ \nu_D \\ \epsilon_w \end{bmatrix} \tag{28}$$

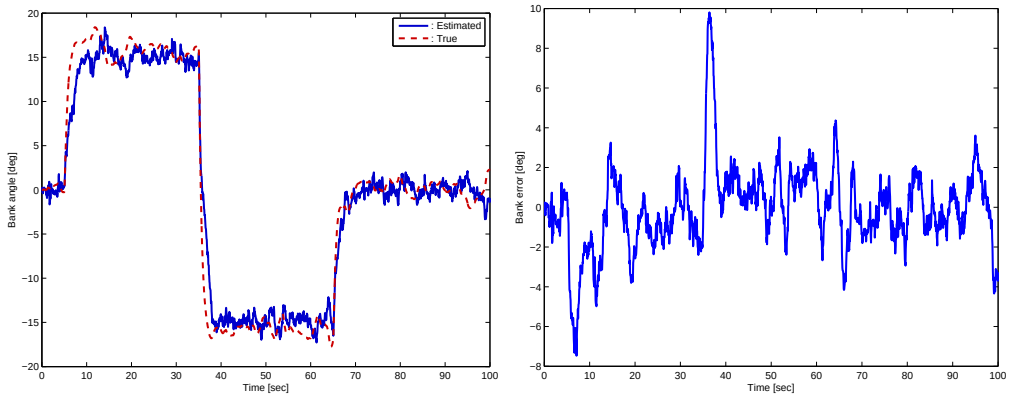

(a) Roll angle filter performance

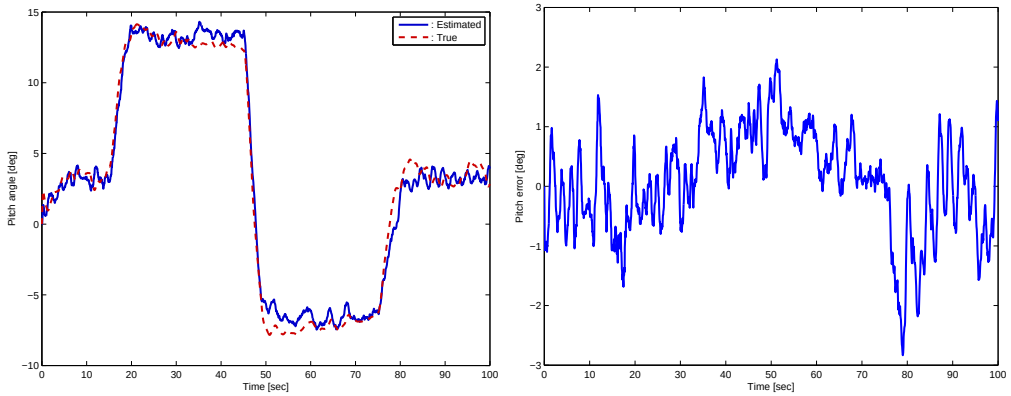

(b) Pitch angle filter performance

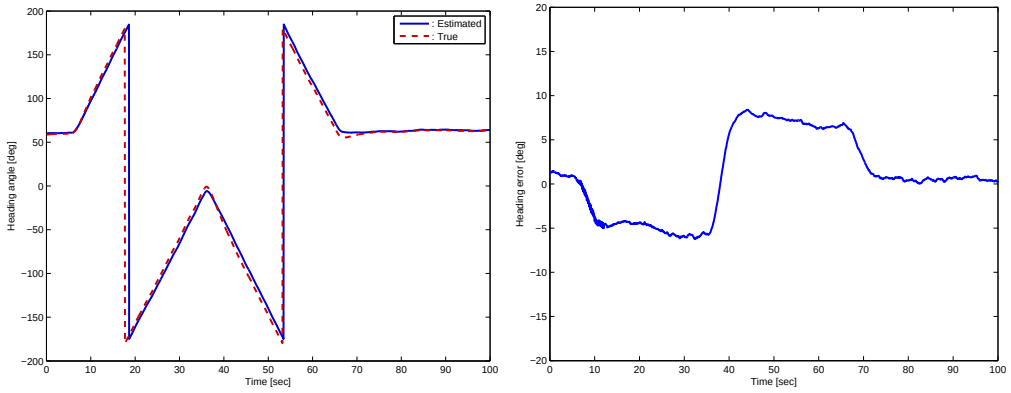

(c) Heading angle filter performance

Figure 7. Attitude filter validation.

where, $[\nu_N \ \nu_E \ \nu_D]^\mathsf{T}$ is the process noise vector of η_w being projected onto the NED frame.

The measurement model for the position estimation filter is described as follows. The North position p_m^N and the East position measurements p_m^E are provided by the GPS sensor at an update rate of 1 Hz,

$$\begin{aligned} p_m^N &= p^N + \eta_N, \\ p_m^E &= p^E + \eta_E, \end{aligned} \tag{29}$$

where η_N and η_E are the measurement noise for the North and East directions, which are assumed to be the Gaussian.

Altitude information with good accuracy is attainable using a barometric altimeter. The one used in our UAV platform has minimum three-meter resolution and a higher update rate. The down position measurement p_m^D with a corresponding Gaussian noise is obtained by,

$$p_m^D = -h + \eta_h. \tag{30}$$

Having multiple measurements at different update rates, the discrete position Kalman filter implementation at a specified sampling period Δt on a micro-controller is given as follows

- **Time update**
  - Project ahead

$$\begin{aligned} \hat{\mathbf{x}}_k^- &= \Phi_k \hat{\mathbf{x}}_{k-1} + V_w[\ \Delta t \sin\hat{\theta}_k \cos\hat{\psi}_k \quad \Delta t \cos\hat{\theta}_k \sin\hat{\psi}_k \quad -\Delta t \sin\hat{\theta}_k \quad 0\ ]^\mathsf{T}, \\ \mathbf{P}_k^- &= \Phi_k \mathbf{P}_{k-1} \Phi_k^\mathsf{T} + \mathbf{Q}_k, \end{aligned} \tag{31}$$

    where,

$$\Phi_k = \begin{bmatrix} 1 & 0 & 0 & -\Delta t \cos\hat{\theta}_k \cos\hat{\psi}_k \\ 0 & 1 & 0 & -\Delta t \cos\hat{\theta}_k \sin\hat{\psi}_k \\ 0 & 0 & 1 & \Delta t \sin\hat{\theta}_k \\ 0 & 0 & 0 & 1 \end{bmatrix}, \qquad \hat{\mathbf{x}}_k = \begin{bmatrix} \hat{p}_k^N \\ \hat{p}_k^E \\ \hat{p}_k^D \\ \hat{V}_{w_k} \end{bmatrix}.$$

- **Measurement update**
  - Compute Kalman gain

$$\mathbf{K}_k = \mathbf{P}_k^- \mathbf{H}_k^{\star\mathsf{T}} \left(\mathbf{H}_k^\star \mathbf{P}_k^- \mathbf{H}_k^{\star\mathsf{T}} + \mathbf{R}_k^\star\right)^{-1}, \tag{32}$$

  - Update estimate with measurements

$$\hat{\mathbf{x}}_k = \hat{\mathbf{x}}_k^- + \mathbf{K}_k(\mathbf{z}_k^\star - \mathbf{H}_k^\star \hat{\mathbf{x}}_k^-), \tag{33}$$

  - Compute error covariance for updated estimate

$$\mathbf{P}_k = (\mathbf{I} - \mathbf{K}_k \mathbf{H}_k^\star)\mathbf{P}_k^-, \tag{34}$$

    where, $\star = s,\ f$.

Each update is performed whenever the corresponding measurement becomes available: a fast update and a slow update.

- Fast update

$$\mathbf{z}_k^f = -h_k, \qquad \mathbf{H}_k^f = [\ 0 \quad 0 \quad 1 \quad 0\ ], \tag{35}$$

- Slow update

$$\mathbf{z}_k^s = \begin{bmatrix} p_{m_k}^N \\ p_{m_k}^E \end{bmatrix}, \qquad \mathbf{H}_k^s = \begin{bmatrix} 1 & 0 & 0 & 0 \\ 0 & 1 & 0 & 0 \end{bmatrix}. \tag{36}$$

The process noise covariance matrix $\mathbf{Q_N}$ and measurement noise covariance matrix $\mathbf{R_N}$ are determined from the noise characteristics of each signal,

$$\begin{aligned} \mathbf{Q_N} &= \text{diag}\Big(E\big[\ \bar{\nu}_N^2 \quad \bar{\nu}_E^2 \quad \bar{\nu}_h^2 \quad \bar{\epsilon}_w^2\ \big]\Big), \\ \mathbf{R}_\mathbf{N}^f &= E\big[\bar{\eta}_h^2\big], \quad \mathbf{R}_\mathbf{N}^s = \text{diag}\Big(E\big[\ \bar{\eta}_N^2 \quad \bar{\eta}_E^2\ \big]\Big), \end{aligned} \tag{37}$$

where the overbar variables represent the discrete noise sequences at a sampling period of Δt having equal noise strength as the continuous noise process, and $E[\cdot]$ calculates the mean-square noise strength.

III.B. Navigation filter validation

The navigation filter was written in C code as an S-function of the Matlab/Simulink® environment, as described in Sec. II.E. The process covariance matrix and the noise covariance matrix for the navigation filter were carefully chosen based on the noise characteristic of the sensors as follows

$$\begin{aligned} \mathbf{Q_N} &= \text{diag}\Big(\big[\ 2^2 \quad 2^2 \quad 2^2 \quad 0.01^2\ \big]\Big), \\ \mathbf{R}_\mathbf{N}^f &= 2^2, \quad \mathbf{R}_\mathbf{N}^s = \text{diag}\Big(\big[\ 3^2 \quad 3^2\ \big]\Big). \end{aligned} \tag{38}$$

An open loop steering command for the UAV to perform an eight-shape maneuver was used, which in turn results in a doublet bank angle command as a reference to the roll PID controller. Figure 8 shows the performance of the navigation filter. Overall, the navigation filter works very well by providing a series of estimation values for the main control loop at a high rate (20 Hz) despite the low update rate of the GPS sensor (1 Hz). The North and East position estimates appear to have certain corrections periodically, which can be explained by the fact that during no GPS output update, the heading estimation from the attitude filters is used to propagate the position estimation. However, the time lag of the heading output from the attitude filters causes the navigation filter to use non ideal heading information during propagation of the states. This results in a drifted position estimate after one second has elapsed when a new GPS measurement becomes available. The navigation Kalman filter works to update the filter states according to the new GPS measurement in order to dump out the drift and to provide the best estimate of position at all times. In addition, the altitude of the UAV is controlled by the altitude PID controller loop along with the doublet reference command, which enables the position filter to be validated with respect to the down position. The Kalman filter works properly at estimating the vertical position despite the noisy barometric altitude measurement.

IV. Experimental Test-bed

The previous attitude and navigation algorithms were implemented on the UAV autopilot described in Ref. 21. The autopilot is built around the Rabbit Semiconductor RCM-3400 micro-controller and it is equipped three single-chip rate gyros, three two-axis accelerometers, a three-axis magnetometer, two pressure sensors, and a GPS receiver. The micro-controller, sensors and associated electronics are integrated on a custom-designed and fabricated four-layer 5" by 3" printed circuit board (PCB), shown in Figure 9.

The micro-controller, a RCM-3400 module from Rabbit semiconductors, features a total of 1 MB code and data memory space and the maximum clock speed at 54 MHz. The memory space allows C programs with over 50,000+ lines of code, and the advanced C compiler with a tightly coded floating-point library is used to generate the executable program that is capable of handling floating-point arithmetic with 7 μsec for floating-point addition and multiplication at the maximum clock speed, which is 20 times faster than other comparable processor unit such as the Intel 386ex® microprocessor.[22] The attitude filter and the navigation filter are cascaded to reduce the computation overhead. Having the minimal dimension of respective filters in conjunction with an explicit formula for matrix inversion, the attitude estimation filters require a computation time of about 10 msec for each sampling period and the navigation Kalman filter requires a computation time of about 3 msec.

Table 1 summarizes the specifications, operational range, resolution, and noise characteristics of the autopilot sensors. Details for the autopilot hardware components and the subsystem integration process can be found in Ref. 21. The autopilot and the corresponding estimation algorithms were tested in a

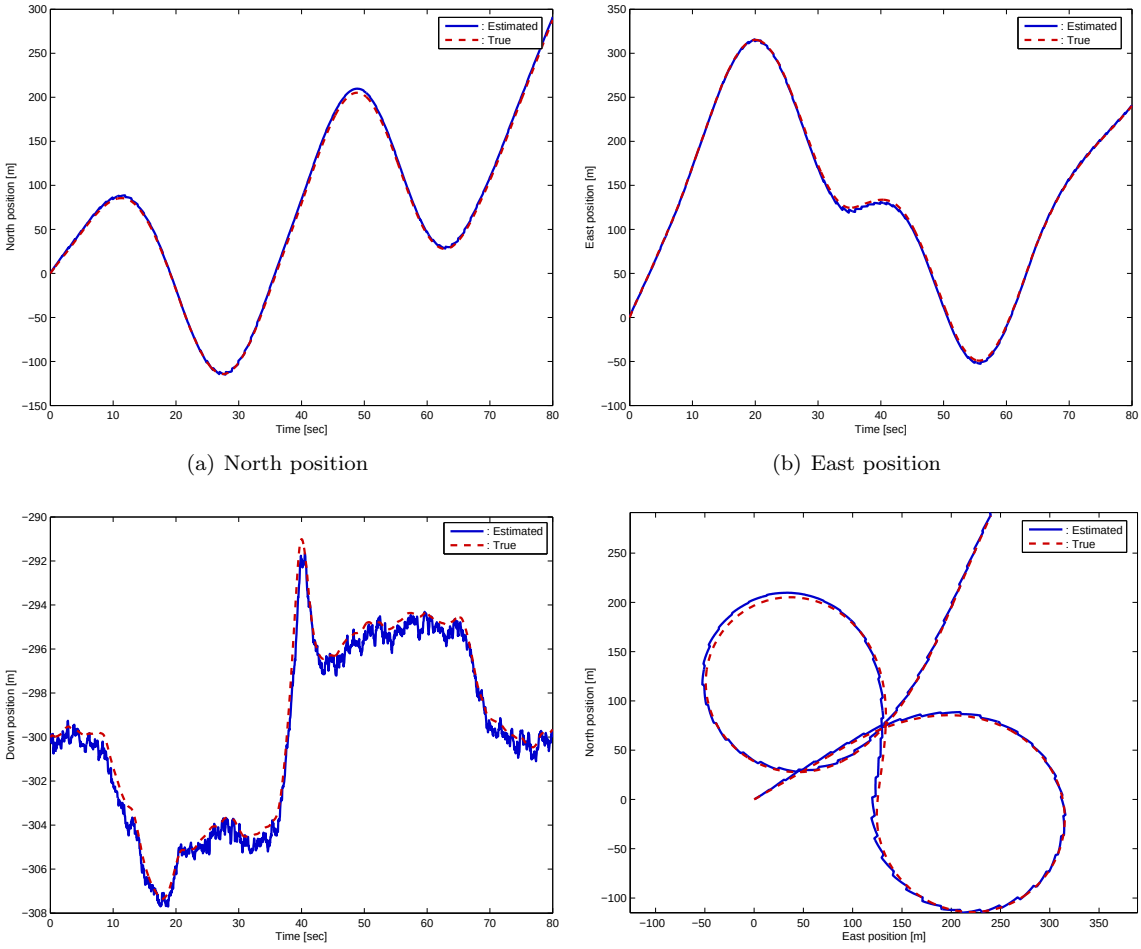

(a) North position

(b) East position

(c) Down position

(d) North-East position

Figure 8. Navigation filter validation.

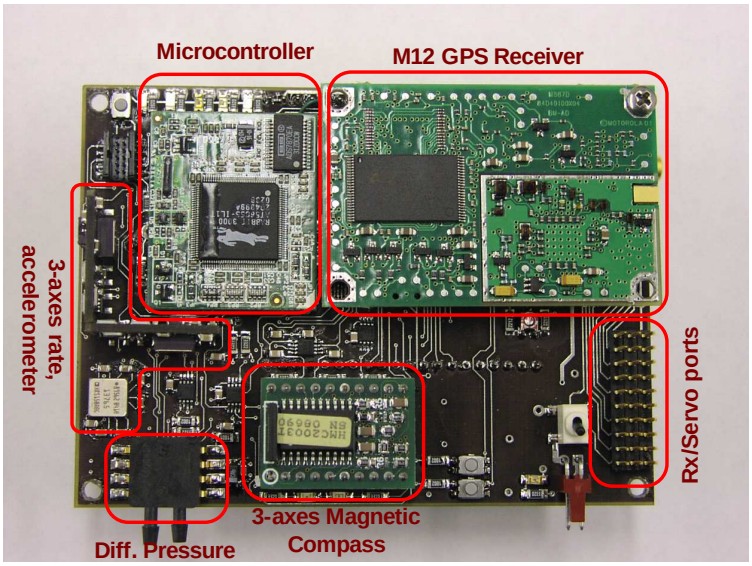

Figure 9. Assembled autopilot hardware.

Table 1. Sensor specifications of autopilot sensors.

Sensors	Range	Resolution	1-σ noise
Accelerometer	± 2 g	0.004 g	0.025 g
Rate gyro	± 150 °/sec	0.1 °/sec	0.4 °/sec
Magnetometer	± 2 gauss	1.22 mgauss	4 mgauss
Absolute pressure	Above sea level	2.75 m	3 m
Differential pressure	79.2 m/sec	1.40 m/sec	1.5 m/sec
Servo Position	± 60 deg	0.5 deg	

hardware-in-the-loop (HIL) environment developed specifically for this purpose. Figure. 10 illustrates the hardware-in-the-loop simulation environment. In the HIL configuration the complete 6-DOF model outputs

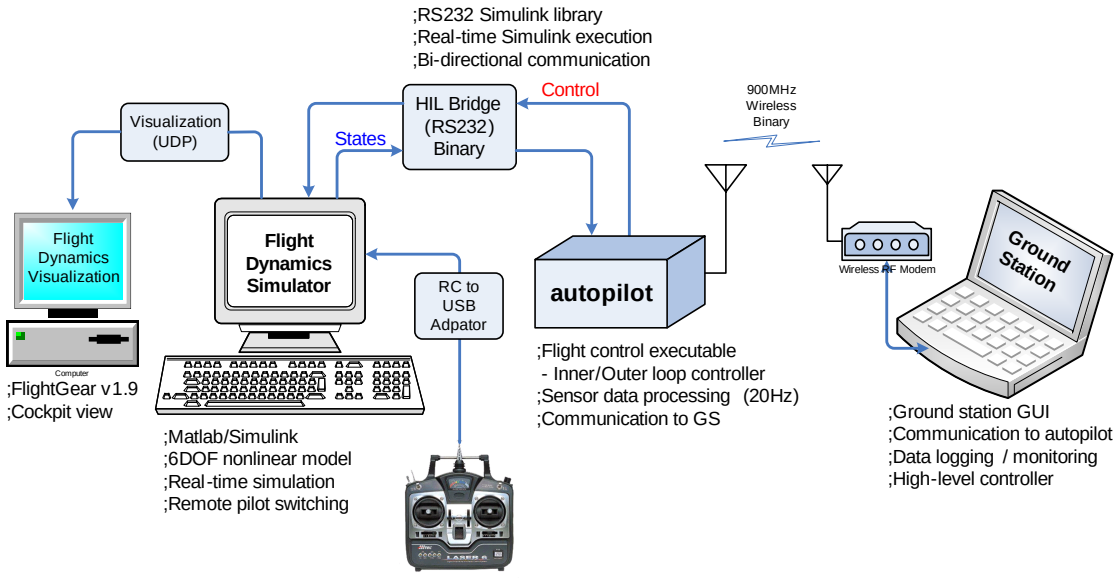

Figure 10. High fidelity hardware-in-the-loop simulation (HILS) environment.

from the simulator are processed to emulate real sensors accounting for sensor latency, random walk bias, and measurement noise. After digitized according to the word size of the micro-controller (12 bit, 4096 steps), the sensor values are transmitted to the autopilot and serve as substitutions for the real sensor measurement. The results from the hardware-in-the-loop validation of the estimation algorithms are similar to the ones shown in Figs. 7-8, which further reveals the fact that the estimation algorithms are suitable for *real-time* control of autonomous small UAVs.

V. Conclusion

A simple, yet effective attitude and position estimation algorithm has been developed for use with a low-cost UAV autopilot. Utilizing a complementary filter for estimating the pitch and heading angles, dramatically reduces the computational burden. A minimal dimension Kalman filter estimates the roll angle. An algorithm for handling GPS lock is given and is tested to show the feasibility of real-time implementation with delayed GPS measurements. A cascaded position filter is also derived, and it is shown to be effective at incorporating the slow GPS output in order to provide a high update rate position solution. Results from both simulation and hardware validation show that this low cost inertial attitude and position reference system is suitable for control of autonomous small UAVs.

Acknowledgment: Partial support for this work has been provided by NSF award CMS-0510259.

References

[1]Psiaki, M. L., "Attiutde-Determination Filtering via Extended Quaternion Estimation," *Journal of Guidance, Dynamics, and Control*, Vol. 23, No. 2, March-April 2000, pp. 206–214.

[2]Marins, J. L., Yun, X., Bachmann, E. R., McGhee, R. B., and Zyda, M. J., "An Extended Kalman Filter for Quaternion-Based Orientation Estimation Using MARG Sensors," *Proceedings of the 2001 IEEE/RSJ International Conference on Intelligent Robots and Systems*, Maui, HW, Oct.-Nov. 2001, pp. 2003–2011.

[3]Choukroun, D., Bar-Itzhack, I. Y., and Oshman, Y., "A Novel Quaternion Kalman Filter," *Proceedings of Guidance, Navigation, and Control Conference*, Monterey, CA, Aug. 2002, AIAA-2002-4460.

[4]Brown, R. G. and Hwang, P. Y. C., *Introduction to Random Signals and Applied Kalman Filtering with Matlab Exercises and Solutions*, John Wiley & Sons, New York, NY, 3rd ed., 1997.

[5]Park, S., *Avionics and Control System Development for Mid-Air Rendezvous of Two Unmanned Aerial Vehicles*, Ph.d. thesis, Massachusetts Institute of Technology, Boston, MA, Feb. 2004.

[6]Shuster, M. D. and Oh, S. D., "Three-Axis Attitude Determination from Vector Observations," *Journal of Guidance, Dynamics, and Control*, Vol. 4, No. 1, Jan.-Feb. 1981, pp. 70–77.

[7]Bachmann, E. R., Yun, X., McKinney, D., McGhee, R. B., and Zyda, M. J., "Design and Implementation of MARG Sensors for 3-DOF Orientation Measurement of Rigid Bodies," *Proceedings of the 2003 IEEE International Conference on Robotics & Automation*, Sept. 2003, pp. 1171–1178.

[8]Crassidis, J. L., Quinn, D. A., Markley, F. L., and McCullough, J. D., "A Novel Sensor for Attitude Determination Using Global Positioning System Signals," *Proceedings of Guidance, Navigation, and Control Conference*, Boston, MA, Aug. 1998, pp. 708–717.

[9]Psiaki, M. L., Powell, S. P., and Jr., P. M. K., "The Accuracy of the GPS-Derived Acceleration Vector, a Novel Attitude Reference," *Proceedings of Guidance, Navigation, and Control Conference*, AIAA, 1999, AIAA-99-4079.

[10]Kornfeld, R. P., Hansman, R. J., Deyst, J. J., Amonlirdvinam, K., and Walker, E. M., "Applications of Global Positioning System Velocity-Based Attitude Information," *Journal of Guidance, Control, and Dynamics*, Vol. 24, No. 5, Sept.-Oct. 2001, pp. 998–1008.

[11]Lee, S., Lee, T., Park, S., and Kee, C., "Flight Test Results of UAV Automatic Control Using a Single-Antenna GPS Receiver," *Proceedings of Guidance, Navigation, and Control Conference*, Austin, Texas, Aug. 2003, AIAA-2003-5593.

[12]Wenger, L. and Gebre-Egziabher, D., "System Concepts and Performance Analysis of Multi-Sensor Navigation Systems for UAV Applications," *Unmanned Unlimited Systems, Technologies, and Operation - Aerospace*, AIAA, San Diego, CA, Sept. 2003, AIAA 2003-6647.

[13]Kingston, D. B. and Beard, R. W., "Real-Time Attitude and Position Estimation for Small UAVs Using Low-Cost Sensors," *AIAA 3rd Unmanned Unlimited Technical Conference, Workshop and Exhibit*, Chicago, IL, Sept. 2004.

[14]Caruso, M. J., "Application of Magnetic Sensors for Low Cost Compass Systems," Honeywell technical article, http://www.ssec.honeywell.com/magnetic/.

[15]Etkin, B. and Reid, L. D., *Dynamics of Flight: Stability and Control*, John Wiley and Sons, New York, NY, 3rd ed., 1996.

[16]Motorola, Inc., *Motorola GPS Products - Oncore User's Guide*, Aug. 2002, Revision 5.0.

[17]Bak, M., Larsen, T., Norgaard, M., Andersen, N., Poulsen, N., and Ravn, O., "Location Estimation using Delayed Measurements," *Proceedings of the 5th International Workshop on Advanced Motion Control (AMC98)*, June-July 1998, pp. 180–185.

[18]Larsen, T., Andersen, N., Ravn, O., and Poulsen, N., "Incorporation of Time Delayed Measurements in a Discrete-time Kalman Filter," *Proceedings of the 37^{th} IEEE Conference on Decision and Control*, Vol. 4, Dec. 1998, pp. 3972–3977.

[19]Jung, D. and Tsiotras, P., "Modelling and Hardware-in-the-loop Simulation for a Small Unmanned Aerial Vehicle," *AIAA Infotech at Aerospace*, Rohnert Park, CA, May 2007, AIAA 07-2763.

[20]Stevens, B. L. and Lewis, F. L., *Aircraft Control and Simulation*, John Wiley & Sons, Hobokren, NJ, 2nd ed., 2003.

[21]Jung, D., Levy, E. J., Zhou, D., Fink, R., Moshe, J., Earl, A., and Tsiotras, P., "Design and Development of a Low-Cost Test-Bed for Undergraduate Education in UAVs," *Proceedings of the 44^{th} IEEE Conference on Decision and Control*, Seville, Spain, Dec. 2005, pp. 2739–2744.

[22]Rabbit Semiconductor, Inc., *Rabbit 3000® Microprocessor User's Manual*, 2003, Part Number 019-0108.